iScience

CellPress
OPEN ACCESS

Article

Lipid Droplets Maintain Energy Homeostasis and Glioblastoma Growth via Autophagic Release of Stored Fatty Acids

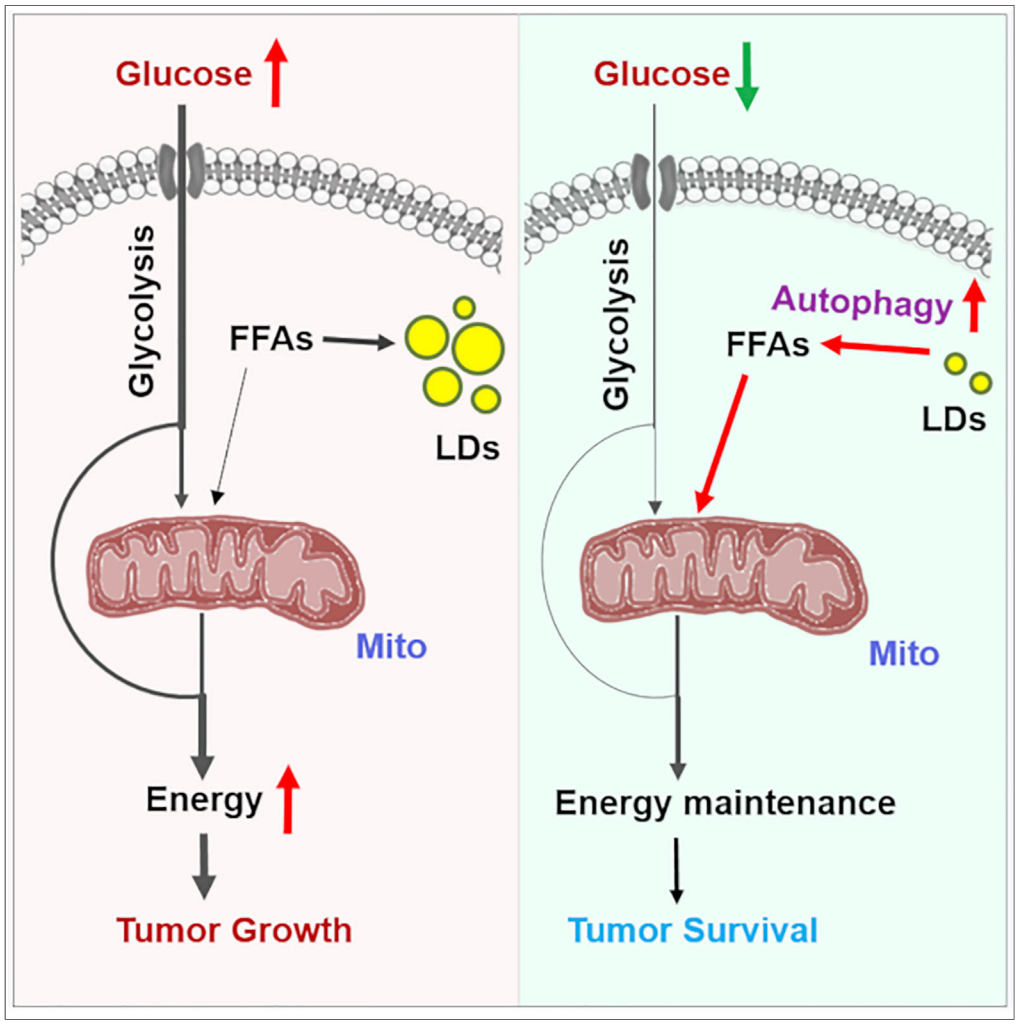

Xiaoning Wu, Feng Geng, Xiang Cheng, ..., William H. Yong, Arnab Chakravarti, Deliang Guo

deliang.guo@osumc.edu

HIGHLIGHTS

TG/LDs function as energy reservoir for GBM tumors

TG/LDs are hydrolyzed by autophagy to maintain GBM survival when glucose levels decrease

TG/LD hydrolysis releases fatty acids that enter into mitochondria for energy production

Inhibiting autophagy causes TG/LD accumulation and GBM cell death

Wu et al., iScience *23*, 101569
October 23, 2020
https://doi.org/10.1016/j.isci.2020.101569

iScience

CellPress
OPEN ACCESS

Article

Lipid Droplets Maintain Energy Homeostasis and Glioblastoma Growth via Autophagic Release of Stored Fatty Acids

Xiaoning Wu,[1,5] Feng Geng,[1,5] Xiang Cheng,[1] Qiang Guo,[1] Yaogang Zhong,[1] Timothy F. Cloughesy,[2] William H. Yong,[3] Arnab Chakravarti,[1] and Deliang Guo[1,4,6,*]

SUMMARY

Recently, lipid metabolism reprogramming has been further evidenced in malignancies via the observation of large amounts of lipid droplets (LDs) in human tumors, including in glioblastoma (GBM), the most lethal primary brain tumor. However, the role played by LDs in tumor cells remains unknown. Here, we show that triglycerides (TG), the major components of LDs, serve as a critical energy reservoir to support GBM cell survival. TG/LDs rapidly diminished in GBM cells upon glucose reduction, whereas inhibiting fatty acid oxidation or autophagy resulted in the accumulation of TG/LDs and strongly potentiated GBM cell death. Immunofluorescence imaging and time-lapse videos showed that LDs are hydrolyzed by autophagy to release free fatty acids that mobilize into mitochondria for energy production. Our study demonstrates that autophagy-mediated hydrolysis of TG/LDs maintains energy homeostasis and GBM survival upon glucose reduction, suggesting that limiting TG/LDs utilization might be necessary upon treating GBM.

INTRODUCTION

Metabolic alteration has been recognized as a hallmark of cancer (Hanahan and Weinberg, 2011; Intlekofer and Finley, 2019), but how lipid metabolism is reprogrammed in tumor cells remains poorly understood. A significant amount of effort has been put into understanding the underlying mechanisms elevating *de novo* fatty acid synthesis and its therapeutic potential in malignancies (Cheng et al., 2015, 2018a, 2018b; Guo, 2016; Guo et al., 2013, 2014; Menendez and Lupu, 2007; Ru et al., 2013; Talebi et al., 2018). However, whether other lipid metabolism pathways are altered in malignancies has not been extensively explored. Recently, our group and several others have found that human tumor tissues exhibit abundant lipid droplets (LDs), including in glioblastoma (GBM), the most lethal primary brain tumor (Cheng et al., 2020; Omuro and DeAngelis, 2013; Wen and Kesari, 2008), and in prostate, pancreas, breast, and clear cell renal cell carcinoma (Accioly et al., 2008; Du et al., 2017; Geng et al., 2016; Geng and Guo, 2017; Mitra et al., 2017; Pucer et al., 2013; Sevinsky et al., 2018; Sunami et al., 2017).

LDs are specific lipids-storage organelles, which are mainly located in adipose tissues (Murphy, 2001; Pond, 1999). A single LD contains a neutral lipid core that comprises triglycerides (TG) and cholesteryl esters, which are surrounded by a monolayer of phospholipid membrane that is associated with multiple proteins (Tauchi-Sato et al., 2002; Walther et al., 2017). A molecule of TG consists of a glycerol molecule with three hydroxyl groups that are each esterified by fatty acids (Olzmann and Carvalho, 2019; Paar et al., 2012). The presence of abundant LDs in cancer cells suggest that storing lipids in tumor tissues may be a common feature of malignancies. However, the role played by LDs in tumor cells is unknown.

In the tumor microenvironment, nutrient supplies are fluctuant due to variation in vascular development (Lyssiotis and Kimmelman, 2017). The mechanism used by tumor cells to solve this challenge and maintain growth has yet to be elucidated. We hypothesized that tumor cells utilize the fatty acids stored in LDs to support their survival and growth upon reduction in nutrient levels. To test this, we investigated the response of GBM cells to glucose deprivation and unveiled that TG/LDs serve as critical energy reservoirs to maintain cell survival upon energetic stress. Furthermore, we showed that GBM cells rapidly break down TG/LDs through an autophagic process that releases their stored fatty acids for energy production when glucose level decreases. Our study suggests that TG/LDs play an important role in the regulation of GBM growth.

[1]Department of Radiation Oncology, James Comprehensive Cancer Center and College of Medicine at the Ohio State University, Columbus, OH 43210, USA

[2]Department of Neurology (Neuro-Oncology), David Geffen School of Medicine at the University of California, Los Angeles, CA 90095, USA

[3]Department of Pathology and Laboratory Medicine (Neuropathology), David Geffen School of Medicine at the University of California, Los Angeles, CA 90095, USA

[4]Center for Cancer Metabolism, James Comprehensive Cancer Center at the Ohio State University, Columbus, OH 43210, USA

[5]These authors contributed equally

[6]Lead Contact

*Correspondence: deliang.guo@osumc.edu

https://doi.org/10.1016/j.isci.2020.101569

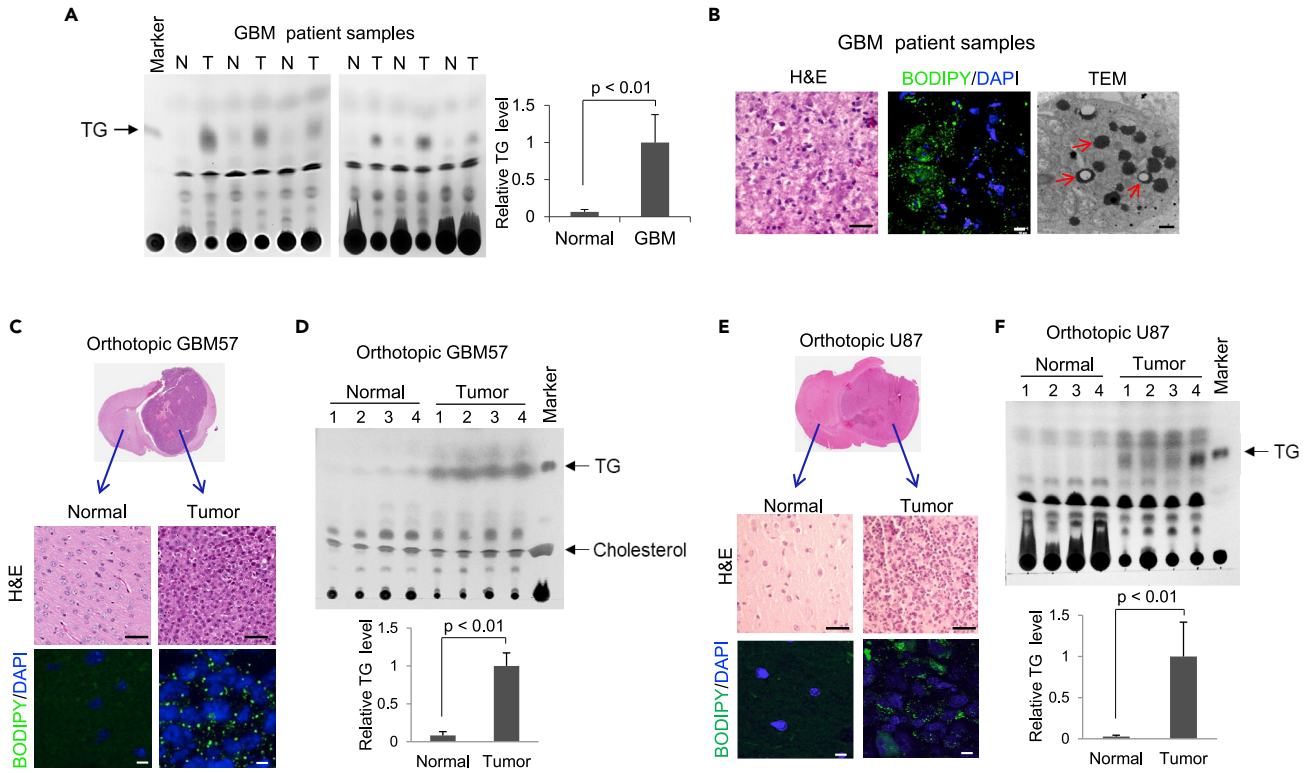

Figure 1. GBM Tumor Tissues Contain Large Amounts of TG and LDs

(A) Thin-layer chromatography (TLC) analysis of total lipid extracts from the same weight (4 mg) of normal (N) versus tumor (T) tissues from GBM patient autopsy samples (middle panel). TG standard loaded on the left. The intensity of TLC TG bands for each sample was quantified by the ImageJ software and normalized to the average intensity of TG in six tumor tissues to determine the relative TG levels between normal brain and GBM tissue (mean ± SD, n = 6) (right panel). Significance was determined by unpaired Student's t test.

(B) Representative images of tumor tissues from GBM patient biopsy stained by H&E (left panel), BODIPY 493/503 (green), and DAPI (blue) (middle panel) or visualized by transmission electron microscopy (TEM) (right panel). Red arrows in TEM image indicate LDs. Scale bar: 50 μm for H&E, 10 μm for fluorescence imaging, 500 nm for TEM.

(C–F) Representative images of normal and tumor tissues from primary GBM57- (C) or U87-derived (E) orthotopic mouse models stained by H&E or BODIPY 493/503 (green)/DAPI (blue). Scale bar: 50 μm for H&E; 10 μm for fluorescence imaging. TLC analysis of total lipid extracts from normal and tumor tissues from GBM57 (D) or U87 (F) orthotopic mice. Relative TG levels were quantified by ImageJ software and normalized to the average TG levels in tumor tissues (mean ± SD, n = 4).

Significance was determined by an unpaired Student's t test. Please also see Figure S1A.

RESULTS

GBM Tissues Contain Large Amounts of TG and LDs

We examined TG levels in paired tumor and normal tissues of autopsy samples from GBM patients using lipid extraction and thin-layer chromatography (TLC). The data show that GBM tumor tissues contained large amounts of TG, which were rarely detected in the contralateral normal brain tissues (Figure 1A), consistent with the prevalence of LDs in GBM tumor tissues (Geng et al., 2016; Geng and Guo, 2017), as observed by confocal microscopy after BODIPY 493/503 staining and transmission electron microscopy (TEM) (Figure 1B). In agreement with these results, GBM patient primary GBM57 cells- or U87 cells-derived orthotopic xenograft models showed that TG/LDs are prominently formed in GBM tumor tissues but rarely formed in normal mouse brain tissues (Figures 1C–1F). In addition, by staining a variety of cancer cell types with BODIPY 493/503, we found that LDs are prevalent in various types of cancer cells, including breast, liver, pancreatic, cervical, skin, and sarcoma cancers (Figure S1A).

Glucose Deprivation Triggers GBM Cells Hydrolyzing TG/LDs to Support Cell Survival

We then investigated whether TG/LDs play a role in supporting GBM cell growth or survival by examining 3 GBM cell lines, i.e., U87, T98, and U251 that contain different amounts of TG (Figures 2A and 2B). Fluorescence imaging shows that U87 cells contain the highest number of LDs compared with the other two cell lines (Figure 2A), consistent with their highest TG levels (Figure 2B). We further compared LDs and TG levels between these 3 GBM cell

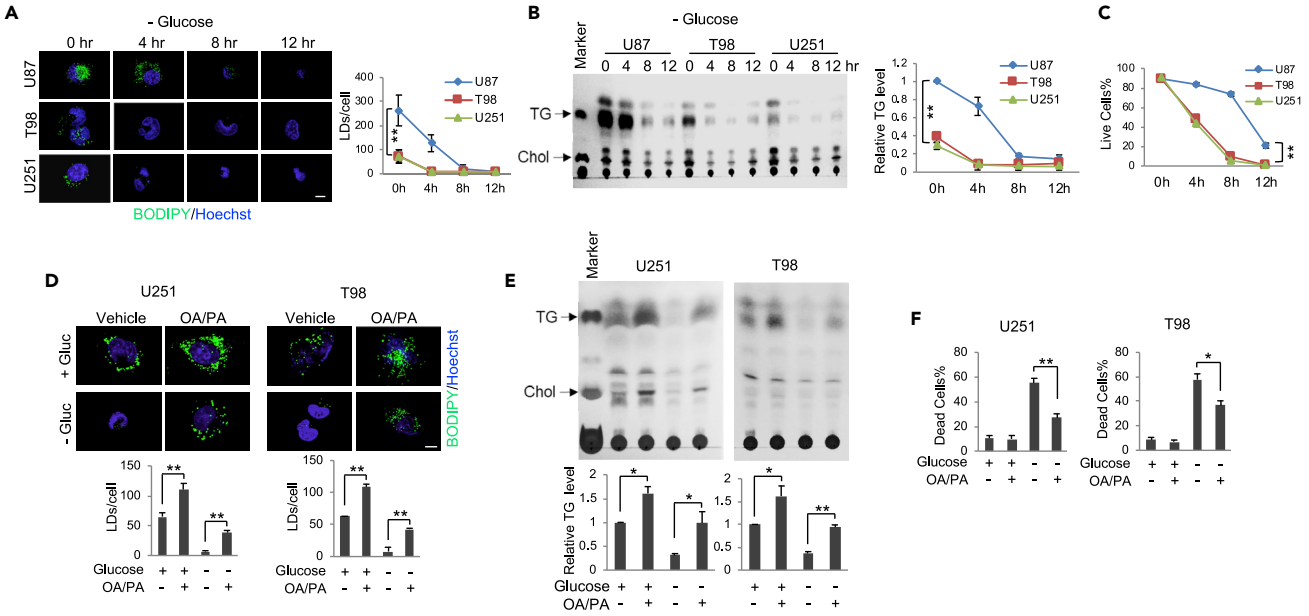

Figure 2. Glucose Deprivation Triggers GBM Cells Hydrolyzing TG/LDs to Support Cell Survival

(A–C) U87, T98, and U251 GBM cells were cultured in medium with 25 mM glucose or no glucose for 4, 8, and 12 h. Cells were stained with BODIPY 493/503 (green)/Hoechst 33342 (blue) and observed by confocal microscopy (A). Quantification of LDs/cell for over 30 cells was conducted using the ImageJ software (mean ± SD). Total lipids were extracted and analyzed by TLC (B). TG levels at different time points and in various cell lines were normalized to U87 cells cultured in 25 mM glucose medium (mean ± SD, n = 3). Live cell percentage at different time points after glucose withdrawal was determined after trypan blue staining (mean ± SD, n = 3) (C). Significance between different cell lines was determined by two-way ANOVA. $^{**}p < 0.001$; $^{*}p < 0.01$. Chol, cholesterol. (D–F) U251 and T98 cells were cultured in medium with/without palmitic acid (PA, C16:0, 5 μM) and oleic acid (OA, C18:1, 5 μM) mixtures (1:1) for 24 h and then placed in fresh medium in the absence or presence of glucose (Gluc, 25 mM) for 4 h. Cells were stained with BODIPY 493/503 (green)/Hoechst 33342 (blue) and observed by confocal microscopy (D). Quantification of LDs/cell in over 30 cells was conducted using ImageJ (mean ± SEM). Total lipid extracts from these cells were analyzed by TLC (E). Relative TG levels were quantified by ImageJ and normalized to the control cells (mean ± SD, n = 3) (E). Cell death was determined by trypan blue exclusion (mean ± SD, n = 3) (F).

Significance was determined by one-way ANOVA. $^{**}p < 0.01$, $^{*}p < 0.05$. Please also see Figure S1B.

lines and transformed astrocytes. The data show that GBM cells have dramatically more LDs and TG than the astrocytes, which are transformed cells that form noticeable amount of LDs/TG (Figure S1B). Whether LDs/TG are formed in normal astrocytes *in vivo* needs further investigation. We then removed glucose from the cell medium to examine the cell response and observed that LDs and TG quickly diminished in all GBM cells within a few hours (Figures 2A and 2B). Through careful examination, we observed that it took 8 h of glucose starvation for LDs and TG present in U87 cells to be greatly reduced, whereas it took only 4 h in T98 and U251 cells where LDs and TG levels are significantly lower (Figures 2A and 2B). Moreover, following the disappearance of TG/LDs, the viability of T98 and U251 cells quickly decreased to around 50% after 4-h glucose starvation and rapidly dropped to ~5% after 8 h (Figures 2C and S1C). In contrast, the reduction of viability in U87 cells was much slower with ~85% viability at 4 h, ~78% at 8 h, and still ~20% at 12 h (Figures 2C and S1C), suggesting that greater TG/LDs levels confer longer GBM cell survival upon glucose starvation.

To validate that TG/LDs can support GBM cell survival, we increased LDs and TG amounts in U251 and T98 cells by supplementing cells with palmitic acid (PA, C16:0) and oleic acid (OA, C18:1) mixtures (1:1) for 24 h before glucose starvation (Figures 2D and 2E). Cells were then placed into fresh media with/without glucose (25 mM) for 4 h. The data show that increasing TG/LDs levels significantly elevated U251 and T98 survival upon glucose starvation as compared with control cells that did not receive PA/OA supplementation (Figures 2D–2F). These data strongly suggest that TG/LDs support GBM cell survival when glucose supply is limited.

TG/LDs Accumulate upon the Inhibition of Fatty Acid β-oxidation under Glucose-free Conditions, Leading to Increased GBM Cell Death

We next examined whether fatty acid β-oxidation plays a role in TG/LDs-supported GBM survival upon glucose starvation. GBM cells were treated with Etomoxir (ETO), an inhibitor of carnitine

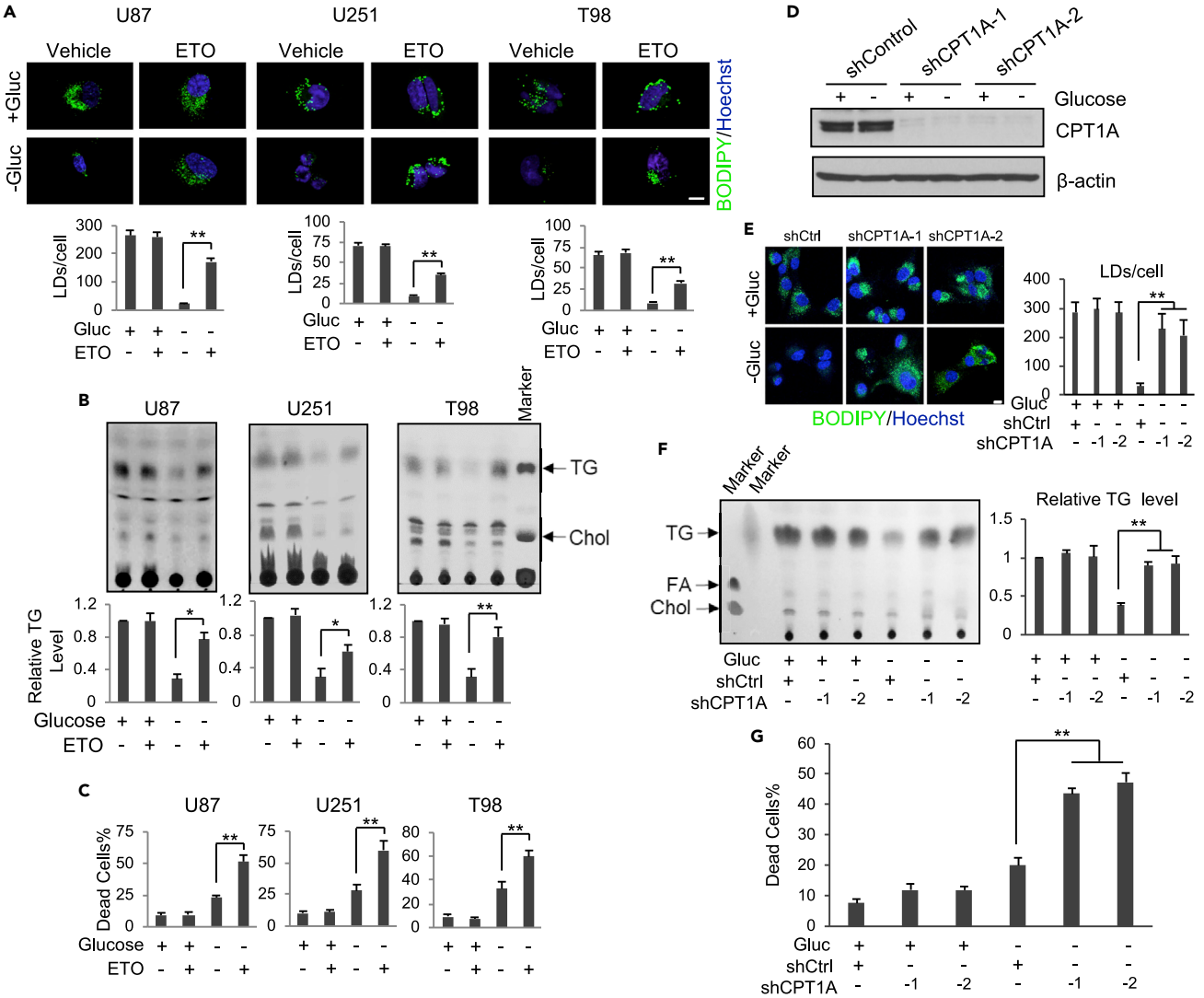

Figure 3. TG/LDs Accumulate upon the Inhibition of Fatty Acid β-Oxidation under Glucose-Free Conditions, Leading to Increased GBM Cell Death

(A and B) Representative fluorescence images of LDs stained with BODIPY 493/503 (green)/Hoechst 33342 (blue) (A). TLC analysis of total lipids (B) in U87 (8 h), U251, and T98 cells (4 h) after treatment with/without ETO (100 μM) in the absence or presence of glucose (25 mM). LDs/cell (mean ± SEM, n = 30) and TG levels (mean ± SD, n = 3) were quantified by ImageJ and normalized to the control cells.

(C) Cell death was determined in U87 (8 h), U251, and T98 cells (3 h) after treatment with/without ETO (100 μM) in the absence or presence of glucose (25 mM) by trypan blue staining (mean ± SD, n = 3).

(D–G) U87 cells were transfected with CPT1A shRNA-expressing lentivirus for 24 h and then cultured in glucose-free or 25 mM glucose medium for 8 h. Cells were analyzed by western blotting (D), observed by confocal microcopy after BODIPY 493/503 and Hoechst 33342 staining (E), or analyzed by TLC for lipid levels (F). LDs/cell (mean ± SEM, n = 30) or relative TG levels (mean ± SD, n = 3) were determined by ImageJ. Cell death was determined after trypan blue staining (mean ± SD, n = 3) (G). FA, fatty acids.

Significance was determined by one-way ANOVA. **p < 0.01, *p < 0.05. Please also see Figure S2.

palmitoyltransferase 1 (CPT1) that transports fatty acids into mitochondria for β-oxidation and energy production (Raud et al., 2018). The data show that under glucose-rich conditions, ETO treatment did not affect LD and TG levels in GBM cells (Figures 3A and 3B) or their survival rate (Figure 3C). In contrast, inhibition of fatty acid oxidation by ETO in the absence of glucose significantly blocked the hydrolysis of LDs and TG (Figures 3A and 3B) and dramatically enhanced GBM cell death (Figure 3C).

We then used a genetic approach to silence CPT1A expression with lentivirus-expressing shRNA and block fatty acid β-oxidation. As with pharmacological inhibition (Figures 3A and 3B), CPT1A knockdown did not affect TG/LDs levels and GBM survival under glucose-rich conditions, but it blocked the hydrolysis

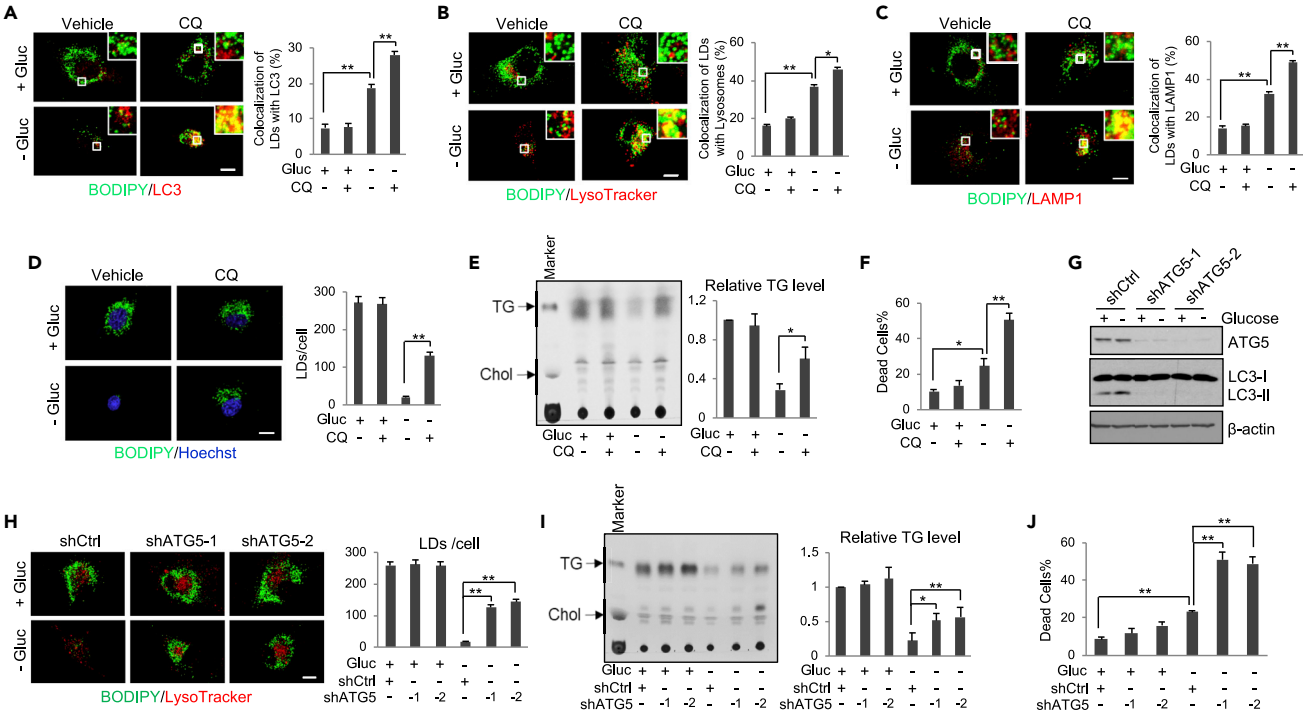

Figure 4. TG/LDs are Hydrolyzed by Autophagy to Support GBM Cell Survival upon Glucose Deprivation

(A) Representative fluorescence images of U87 cells stained with BODIPY 493/503 (green) and anti-LC3 antibody (red) in the absence or presence of glucose (25 mM) and chloroquine (CQ, 5 μM) for 6 h. The co-localization was quantified by ImageJ (mean ± SEM) in over 30 cells.

(B and C) Representative fluorescence images of U87 cells co-stained with BODIPY 493/503 (green) and LysoTracker (red) (B) or anti-LAMP1 antibody (red) (C) in the presence or absence of glucose (25 mM) and CQ (5 μM) for 6 h. The co-localization was quantified by ImageJ (mean ± SEM, n = 30).

(D–F) Representative fluorescence images of U87 cells stained with BODIPY 493/503 (green) and Hoechst 33342 (blue) in the absence or presence of glucose (25 mM) and CQ (5 μM) for 8 h. LDs/cell were quantified in 30 cells (mean ± SEM, n = 30) (D). Their total lipids were analyzed by TLC (mean ± SD, n = 3) (E). Cell death was determined after trypan blue staining (mean ± SD, n = 3) (F).

(G–J) U87 cells were transfected with ATG5 shRNA-expressing lentivirus for 24 h and then cultured in medium without/with glucose (25 mM) for 8 h. Cell lysates were subjected to western blotting analysis using the indicated antibodies (G). Cells were stained with BODIPY 493/503 (green) and LysoTracker (red) and observed by confocal microscopy (H). Total cellular lipids were analyzed by TLC (I). Cell death was determined after trypan blue staining (J). Quantification and significance determination of LD number, relative TG levels, and cell death were same as in panels D–F.

Statistical significance was determined by one-way ANOVA for this entire figure; $^{**}p < 0.01$, $^{*}p < 0.05$. Please also see Figures S3 and S4, and Videos S1, S2, S3, and S4.

of TG/LDs induced by glucose starvation (Figures 3D–3F, S2A and S2B) and significantly elevated GBM cell death (Figures 3G and S2C).

TG/LDs Are Hydrolyzed by Autophagy to Support GBM Cell Survival upon Glucose Starvation

We next examined how TG/LDs are hydrolyzed in GBM cells upon glucose starvation. Western blotting showed that autophagy is induced by glucose starvation in GBM cells, as demonstrated by an increase of the LC3 lipidation band (lower band, LC3-II), a marker of autophagosome formation (Kabeya et al., 2000) (Figure S3A). We then co-stained LDs and autophagosomes with BODIPY 493/503 (green) and anti-LC3 antibody (red). The data show that glucose starvation significantly increased the co-localization of LDs with LC3-stained autophagosomes, which was more prominent when lysosomal activity was suppressed by chloroquine (CQ) (Figure 4A), a lysotropic drug that reduces lysosomal acidification and thereby suppresses the activities of lysosomal hydrolases (Amaravadi et al., 2007; Mauthe et al., 2018). Moreover, using stably expressing red fluorescent protein (RFP)-LC3 U251 cells and time-lapse videos, we observed that glucose starvation, but not glucose-rich conditions, induces the direct association of LDs and RFP-LC3-labeled autophagosomes (Videos S1 and S2).

We then examined whether TG/LDs are hydrolyzed in lysosomes. We co-stained LDs and lysosomes with BODIPY 493/503 (green) and LysoTraker (red) in U87 cells after glucose starvation for 6 h. Live cell imaging and time-

lapse video demonstrated that glucose starvation dramatically induced the mobilization of LDs into the lysosomes for hydrolysis (Figures 4B and S3B and Videos S3 and S4). The co-localization of LDs and lysosomes was more prominent when lysosomal activity was suppressed by CQ under glucose-poor conditions (Figure 4B). Co-localization was further confirmed by immunofluorescence staining of lysosomal-associated membrane protein 1 (LAMP1) together with LD staining by BODIPY 493/503 (Figure 4C). Accordingly, inhibition of lysosomal activity by CQ or the specific inhibitor of vacuolar H + ATPase that controls lysosomal acidification, bafilomycin (Mauvezin and Neufeld, 2015), blocked the hydrolysis of LDs and TG triggered by glucose starvation (Figures 4D, 4E, S4A, S4B, and S4D), resulting in a significant increase of GBM cell death (Figures 4F, S4C, and S4E), which was reduced by supplementing the media with OA/PA (Figure S4C). Moreover, we examined the effects of glucose starvation in neurospheres from GBM-patient-derived primary GBM83 cells. Similar as in U87 cells, confocal microscopy imaging showed that glucose starvation in GBM83 cells promoted the co-locolization of LDs with LC3-stained autophagosomes and LysoTracker-stained lysosomes (Figures S4F and S4G), and CQ treatment resulted in LD accumulation (Figure S4H).

We next genetically silenced the expression of ATG5 (Figure 4G), the key gene controlling autophagosome formation (Mizushima et al., 1998), to confirm the role of autophagy in TG/LDs hydrolysis. Western blotting showed that knockdown of ATG5 using lentivirus-mediated shRNA dramatically blocked the lipidation of LC3 (LC3-II) in GBM cells (Figure 4G), demonstrating the blockade of the autophagic process by ATG5 silencing. Moreover, ATG5 knockdown prominently suppressed glucose-deprivation-induced TG/LDs hydrolysis (Figures 4H and 4I), and significantly increased GBM cell death (Figure 4J), demonstrating that TG/LDs are hydrolyzed by autophagy to support GBM survival.

LD-Stored Fatty Acids Released by Autophagy Move into Mitochondria for Energy Production

We next examined the mobilization of fatty acids released from LDs. We first used BODIPY-labeled palmitic acid (BODIPY-PA, green) to culture U87 cells to form fluorescently labeled LDs (Figure 5A, left panel). After 12-h cultures, BODIPY-PA entered the cells and was stored into LDs (green dots), which were stained by Nile red, a fluorescent dye that stains neutral lipids and LDs (Figure 5A, middle and right panels). Moreover, BODIPY-PA-labeled LDs co-stained with TIP47, a specific LD membrane protein (Geng et al., 2016) (Figure 5B). These data demonstrate that BODIPY-labeled PA was stored in LDs in GBM cells. We then washed the cells with PBS to remove free BODIPY-PA and placed these cells into glucose-rich (25 mM) or glucose-free media for 8 h in the presence or absence of CQ or ETO. The cells were then stained with MitoTracker (red) to visualize the mitochondria. Under glucose-rich conditions, fluorescence imaging showed that BODIPY-labeled PA remained within LDs and did not move into the mitochondria and that CQ or ETO treatment had no effect (Figure 5C, left panels). In contrast, after glucose withdrawal for 8 h, green-labeled LDs were rapidly broken down and BODIPY-labeled PA diffused into the cytosol and trafficked into the mitochondria (Figure 5C, right panels), as demonstrated by the greatly increased co-localization of BODIPY-PA and MitoTracker-labeled mitochondria (Figure 5C, right and left panels). Blocking lysosomal activity by CQ or blocking fatty acid oxidation with ETO strongly suppressed glucose-starvation-induced breakdown of LDs and inhibited BODIPY-PA moving into the mitochondria (Figure 5C).

We then used a genetic approach to confirm that the trafficking of BODIPY-PA from LDs to mitochondria is mediated by autophagy. We first infected U87 cells with shRNA-expressing lentivirus for 24 h to knockdown ATG5 or CPT1A and then cultured these cells with BODIPY-labeled PA for an additional 12 h. The cells were then washed with PBS and placed in fresh medium in the presence (25 mM) or absence of glucose for 8 h. As shown in Figure 5D, BODIPY-labeled PA remained within the LDs in GBM cells infected with scramble shRNA and in ATG5 and CPT1A knockdown cells under glucose-rich conditions (Figure 5D, left panels). In contrast, glucose withdrawal induced the breakdown of LDs and promoted BODIPY-PA diffusing into the cytosol and trafficking into mitochondria in control-shRNA-infected cells (Figure 5D, right panels), whereas inhibition of autophagy by ATG5 knockdown or blocking fatty acid oxidation via CPT1A silencing dramatically suppressed LD hydrolysis and blocked BODIPY-PA trafficking from LDs into mitochondria (Figure 5D, right panels). Taken together, these results demonstrate that LD-stored fatty acids are released by autophagy and then move into mitochondria for β-oxidation upon glucose starvation in GBM cells.

DISCUSSION

In the past decade, metabolic reprogramming in cancer cells has been extensively investigated; however, the identification of effective metabolic targets for cancer therapy has only incrementally progressed. In

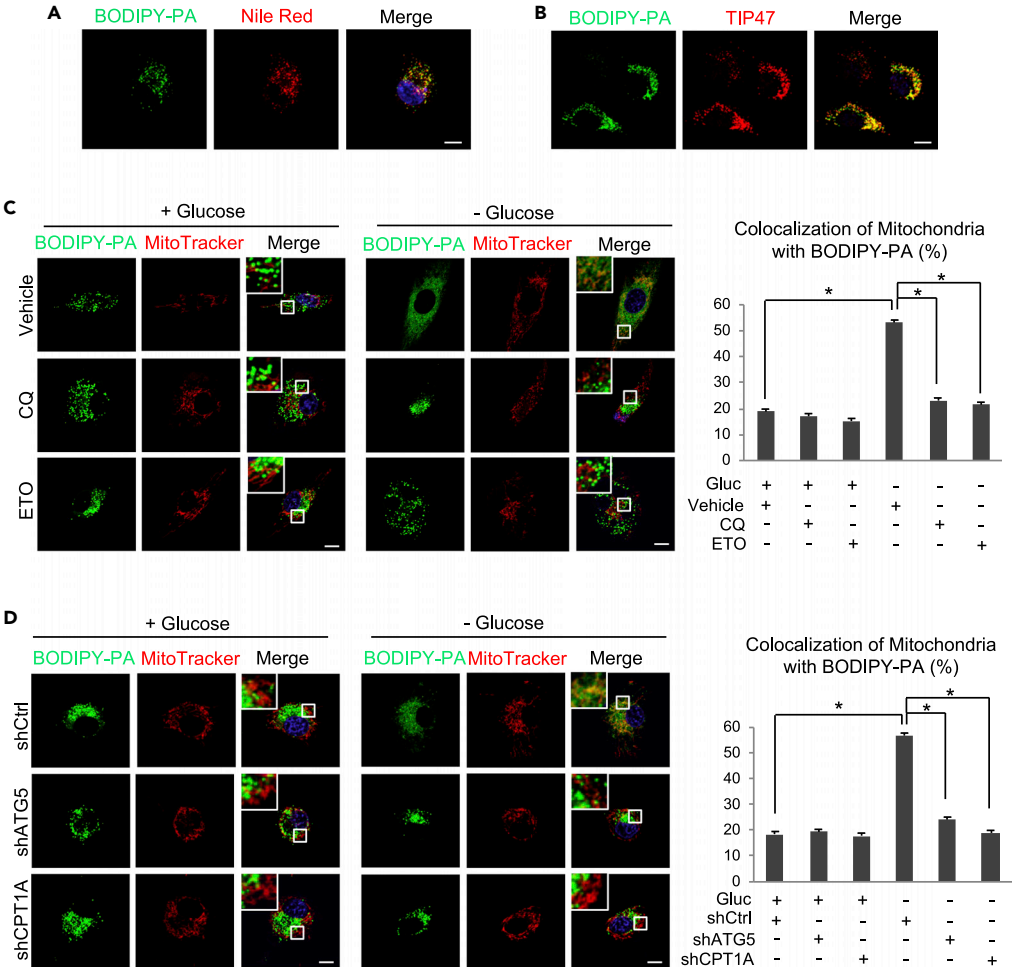

Figure 5. LD-Stored Fatty Acids Released by Autophagy Move into Mitochondria for Energy Production

(A and B) Representative fluorescence images of U87 cells after culturing with BODIPY-labeled PA (C16:0; Cat# D3821, Life Technologies) (0.5 μM) for 12 h and then staining with Nile red and Hoechst 33342 (blue) (A) or with anti-TIP47 antibody (red) (B). Scale bar: 10 μm.

(C) U87 cells were cultured with BODIPY-PA (0.5 μM) for 12 h and then treated with/without CQ (5 μM) or ETO (100 μM) in the absence or presence of glucose (25 mM) for 8 h. Cells were then stained with MitoTracker (Red) and Hoechst 33342 (blue) and visualized by confocal microscopy. The co-localization of diffused BODIPY-PA and mitochondria was determined by the ratio of co-localized red and green signal (yellow) to total red signal using the ImageJ software (mean ± SEM, n = 30). Significance was determined by one-way ANOVA. *$p < 0.01$.

(D) U87 cells were transfected with shRNA-expressing lentivirus against ATG5 or CPT1A for 24 h and then cultured with BODIPY-labeled PA (0.5 μM) for 12 h. Cells were then placed into fresh medium without/with glucose (25 mM) for 8 h. Cell staining and quantification of the co-localization of BODIPY-PA and mitochondria were the same as in Panel C. Significance was determined by one-way ANOVA. *$p < 0.01$.

this study, we show that TG/LDs, functioning as critical energy reservoirs, support GBM cell survival when glucose supply decreases (Figure 6). We demonstrate that TG/LDs are hydrolyzed by autophagy to release their stored fatty acids for energy production and support GBM cell survival upon glucose starvation, suggesting that blocking TG/LDs utilization may be necessary upon targeting GBM (Figure 6).

In the tumor microenvironment, nutrient supplies are frequently scarce due to the poor vascularization (Wellen and Thompson, 2010). Our results show that GBM cells promptly utilize TG/LDs to provide abundant fatty acids for energy production upon glucose starvation, demonstrating the high plasticity and resilience of malignant cells at times of energetic stress. It has been shown that GBM cells have developed efficient machineries to quickly import nutrients and synthesize macromolecules (Cosset et al., 2017; Flavahan et al., 2013; Geng et al., 2016; Guo et al., 2009,

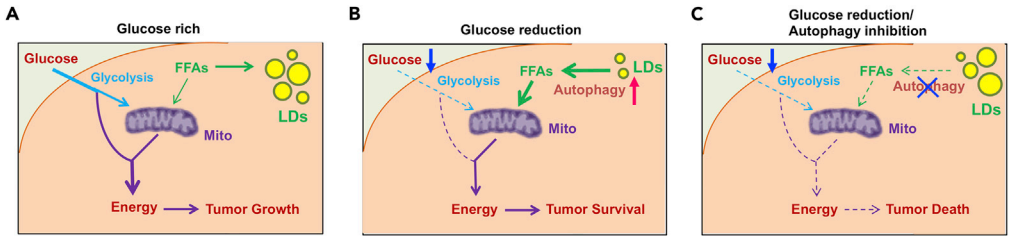

Figure 6. Schematic Model of TG/LDs Hydrolysis Mediated by Autophagy, Maintaining GBM Cell Energy Homeostasis and Survival

(A–C) GBM cells maintain energy homeostasis by utilizing glucose and TG/LDs. Under glucose-rich conditions, GBM cells mainly use glucose for energy production (A). Upon glucose starvation, autophagy is activated, which breaks down TG/LDs and releases the stored fatty acids that enter mitochondria for energy production (B). Blocking TG/LDs hydrolysis via inhibiting autophagy upon glucose reduction conditions will induce dramatic GBM cell death (C).

2011; Vlashi et al., 2011). Under nutrient-rich conditions, GBM cells can absorb abundant glucose, which is converted to fatty acids that are then stored into LDs when in excess. Upon external nutrient paucity, we showed that GBM cells induced LDs breakdown and TG hydrolysis via autophagy (Figure 6). Autophagy is a critical cellular process that degrades protein aggregates and damaged organelles and recycles nutrients by hydrolyzing cytoplasmic components, thereby maintaining cellular homeostasis (Klionsky and Emr, 2000; Mizushima and Komatsu, 2011; Mizushima et al., 2008). Given the importance of autophagy in mediating the turnover of cytoplasmic components, autophagy has been shown to be one of the cellular defense mechanisms under nutrient stress (Komatsu et al., 2005; Lee et al., 2014). The first study showing a link between LDs and autophagy was in hepatic cells, which suggested that autophagy played a critical role in LD hydrolysis (Singh et al., 2009). A later study showed that chaperone-mediated autophagy can degrade LD-associated proteins, perilipin 2 (PLIN2) and perilipin 3 (PLIN3), and facilitate LD breakdown in mice livers upon nutrient shortage (Kaushik and Cuervo, 2015). However, the interaction between LDs and autophagy has not been reported in tumor tissues, and its role in human cancer is unclear. Our data showed that GBM cells can utilize autophagy to quickly hydrolyze TG/LDs to release fatty acids, demonstrating the importance of autophagy in maintaining energy homeostasis by hydrolyzing internally stored lipids. Thus, identifying an approach to block the utilization of LDs-stored fatty acids could be an effective strategy to inhibit GBM growth.

GBM is the most lethal brain tumor and is a very difficult cancer to treat (Omuro and DeAngelis, 2013; Wen and Kesari, 2008), with a median survival of only about 15 months after initial diagnosis despite extensive therapies (Stupp et al., 2009; Wen and Kesari, 2008). The greatest challenge in treating GBM is the unavoidable resistance to treatments developed by tumor cells (Bao et al., 2006; Nguyen et al., 2018). The standard therapy for GBM is radiation together with chemotherapy after surgery (Weller et al., 2014). Resistance to these treatments requires tumor cells to quickly repair their damaged DNA, which consumes large amounts of energy (Aird et al., 2015; Brace et al., 2016). Our data show that GBM cells can rapidly break down TG/LDs by autophagy for energy production. Given that radiation and chemotherapies have been shown to induce autophagy in GBM cells (Chaurasia et al., 2016; Classen et al., 2019; Jiang et al., 2017, 2019), we speculate that TG/LDs via autophagy contribute great amounts of energy to support GBM resistance to these therapies. Thus, blocking TG/LDs breakdown might increase GBM sensitivity to treatments and overcome resistance. Further studies are needed that should explore whether combining radiation and chemotherapies with blockade of TG/LDs utilization could effectively reduce resistance and suppress GBM growth.

Recent studies have shown that LDs are being formed in various cancers, including breast, prostate, and clear renal cell carcinoma among others (Accioly et al., 2008; Du et al., 2017; Geng et al., 2016; Mitra et al., 2017; Pucer et al., 2013; Sevinsky et al., 2018; Sunami et al., 2017). Autophagic release of LDs-stored fatty acids is highly likely to occur in different cancer types, which may be a common mechanism to support tumor cell survival upon nutrient reduction. Our study identifying the role of TG/LDs in maintaining energy homeostasis via autophagy will have a broad impact on cancers other than GBM. Therefore, it will be important in the future to further explore the role of LDs in different cancers, as targeting TG/LDs hydrolysis may be an effective means to sensitize tumor cells to therapies in a variety of cancer types.

Limitations of the Study

Our study unveiled the critical bioenergetic role played by TG/LDs in GBM cells and demonstrated that autophagy mediates TG/LD hydrolysis, also named lipophagy, to release their stored fatty acids for energy

production. Nevertheless, the study was mainly performed *in vitro* in GBM cell lines, although multiple cell lines were examined. Future research needs to include *in vivo* studies to validate the bioenergetic role of TG/LDs in GBM and to demonstrate autophagic hydrolysis of TG/LDs in tumor tissues. In addition, how the autophagy machinery can specifically recognize and target LDs to hydrolyze TG remains unknown. Certainly, further research is needed to fully uncover the function and regulation of TG/LDs in human cancers.

Resource Availability

Lead Contact

Further information and requests for resources and materials should be directed to and will be fulfilled by the Lead Contact, Deliang Guo (deliang.guo@osumc.edu).

Materials Availability

All reagents generated in this study are available from the Lead Contact without restriction.

Data and Code Availability

This study did not generate/analyze datasets or computer code/algorithm.

METHODS

All methods can be found in the accompanying Transparent Methods supplemental file.

SUPPLEMENTAL INFORMATION

Supplemental Information can be found online at https://doi.org/10.1016/j.isci.2020.101569.

ACKNOWLEDGMENTS

This work was supported by NINDS and NCI grants NS104332, NS112935 and R01CA240726 to DG, CA227874 to DG/AC, and American Cancer Society Research Scholar Grant RSG-14-228-01–CSM to DG. TFC and WHY are supported in part by the UCLA SPORE in Brain Cancer (NIH/NCI 1P50CA211015-01A1) and the Art of the Brain Foundation. We also appreciate the support from OSUCCC-Pelotonia Idea grant and start-up funds to DG. The authors wish to thank Dr. Martine Torres for her editorial assistance.

AUTHOR CONTRIBUTIONS

D.G. conceived the ideas. X.W., F.G., and D.G. designed the experiments. X.W., F.G., X.C., Q.G., and Y.Z. performed the experiments. X.W., F.G., X.C., A.C., and D.G. analyzed the data. W.Y. and T.C. procured and provided normal brain and GBM autopsy samples. X.W. and D.G. wrote the manuscript, and all authors reviewed and approved the manuscript for publication.

DECLARATION OF INTERESTS

The authors declare that there are no conflicts of interest for this manuscript.

Received: May 11, 2020
Revised: August 18, 2020
Accepted: September 14, 2020
Published: October 23, 2020

REFERENCES

Accioly, M.T., Pacheco, P., Maya-Monteiro, C.M., Carrossini, N., Robbs, B.K., Oliveira, S.S., Kaufmann, C., Morgado-Diaz, J.A., Bozza, P.T., and Viola, J.P. (2008). Lipid bodies are reservoirs of cyclooxygenase-2 and sites of prostaglandin-E2 synthesis in colon cancer cells. Cancer Res. *68*, 1732–1740.

Aird, K.M., Worth, A.J., Snyder, N.W., Lee, J.V., Sivanand, S., Liu, Q., Blair, I.A., Wellen, K.E., and Zhang, R. (2015). ATM couples replication stress and metabolic reprogramming during cellular senescence. Cell Rep. *11*, 893–901.

Amaravadi, R.K., Yu, D., Lum, J.J., Bui, T., Christophorou, M.A., Evan, G.I., Thomas-Tikhonenko, A., and Thompson, C.B. (2007). Autophagy inhibition enhances therapy-induced apoptosis in a Myc-induced model of lymphoma. J. Clin. Invest. *117*, 326–336.

Bao, S., Wu, Q., McLendon, R.E., Hao, Y., Shi, Q., Hjelmeland, A.B., Dewhirst, M.W., Bigner, D.D., and Rich, J.N. (2006). Glioma stem cells promote radioresistance by preferential activation of the DNA damage response. Nature *444*, 756–760.

Brace, L.E., Vose, S.C., Stanya, K., Gathungu, R.M., Marur, V.R., Longchamp, A., Trevino-Villarreal, H., Mejia, P., Vargas, D., Inouye, K., et al. (2016). Increased oxidative phosphorylation in

response to acute and chronic DNA damage. NPJ Aging Mech. Dis. *2*, 16022.

Chaurasia, M., Bhatt, A.N., Das, A., Dwarakanath, B.S., and Sharma, K. (2016). Radiation-induced autophagy: mechanisms and consequences. Free Radic. Res. *50*, 273–290.

Cheng, C., Geng, F., Cheng, X., and Guo, D. (2018a). Lipid metabolism reprogramming and its potential targets in cancer. Cancer Commun. (Lond). *38*, 27.

Cheng, X., Li, J., and Guo, D. (2018b). SCAP/SREBPs are central players in lipid metabolism and novel metabolic targets in cancer therapy. Curr. Top. Med. Chem. *18*, 484–493.

Cheng, C., Ru, P., Geng, F., Liu, J., Yoo, J.Y., Wu, X., Cheng, X., Euthine, V., Hu, P., Guo, J.Y., et al. (2015). Glucose-mediated N-glycosylation of SCAP is essential for SREBP-1 activation and tumor growth. Cancer Cell *28*, 569–581.

Cheng, X., Geng, F., Pan, M., Wu, X., Zhong, Y., Wang, C., Tian, Z., Cheng, C., Zhang, R., Puduvalli, V., et al. (2020). Targeting DGAT1 ameliorates glioblastoma by increasing fat catabolism and oxidative stress. Cell Metab. *32*, 229–242 e228.

Classen, F., Kranz, P., Riffkin, H., Pompsch, M., Wolf, A., Gopelt, K., Baumann, M., Baumann, J., Brockmeier, U., and Metzen, E. (2019). Autophagy induced by ionizing radiation promotes cell death over survival in human colorectal cancer cells. Exp. Cell Res. *374*, 29–37.

Cosset, E., Ilmjarv, S., Dutoit, V., Elliott, K., von Schalscha, T., Camargo, M.F., Reiss, A., Moroishi, T., Seguin, L., Gomez, G., et al. (2017). Glut3 addiction is a druggable vulnerability for a molecularly defined subpopulation of glioblastoma. Cancer Cell *32*, 856–868.e855.

Du, W., Zhang, L., Brett-Morris, A., Aguila, B., Kerner, J., Hoppel, C.L., Puchowicz, M., Serra, D., Herrero, L., Rini, B.I., et al. (2017). HIF drives lipid deposition and cancer in ccRCC via repression of fatty acid metabolism. Nat. Commun. *8*, 1769.

Flavahan, W.A., Wu, Q., Hitomi, M., Rahim, N., Kim, Y., Sloan, A.E., Weil, R.J., Nakano, I., Sarkaria, J.N., Stringer, B.W., et al. (2013). Brain tumor initiating cells adapt to restricted nutrition through preferential glucose uptake. Nat. Neurosci. *16*, 1373–1382.

Geng, F., Cheng, X., Wu, X., Yoo, J.Y., Cheng, C., Guo, J.Y., Mo, X., Ru, P., Hurwitz, B., Kim, S.H., et al. (2016). Inhibition of SOAT1 suppresses glioblastoma growth via blocking SREBP-1-mediated lipogenesis. Clin. Cancer Res. *22*, 5337–5348.

Geng, F., and Guo, D. (2017). Lipid droplets, potential biomarker and metabolic target in glioblastoma. Intern. Med. Rev. (Wash D C) *3*, https://doi.org/10.18103/imr.v3i5.443.

Guo, D. (2016). SCAP links glucose to lipid metabolism in cancer cells. Mol. Cell Oncol. *3*, e1132120.

Guo, D., Bell, E.H., and Chakravarti, A. (2013). Lipid metabolism emerges as a promising target for malignant glioma therapy. CNS Oncol. *2*, 289–299.

Guo, D., Bell, E.H., Mischel, P., and Chakravarti, A. (2014). Targeting SREBP-1-driven lipid metabolism to treat cancer. Curr. Pharm. Des. *20*, 2619–2626.

Guo, D., Prins, R.M., Dang, J., Kuga, D., Iwanami, A., Soto, H., Lin, K.Y., Huang, T.T., Akhavan, D., Hock, M.B., et al. (2009). EGFR signaling through an Akt-SREBP-1-dependent, rapamycin-resistant pathway sensitizes glioblastomas to antilipogenic therapy. Sci. Signal. *2*, ra82.

Guo, D., Reinitz, F., Youssef, M., Hong, C., Nathanson, D., Akhavan, D., Kuga, D., Amzajerdi, A.N., Soto, H., Zhu, S., et al. (2011). An LXR agonist promotes glioblastoma cell death through inhibition of an EGFR/AKT/SREBP-1/LDLR-dependent pathway. Cancer Discov. *1*, 442–456.

Hanahan, D., and Weinberg, R.A. (2011). Hallmarks of cancer: the next generation. Cell *144*, 646–674.

Intlekofer, A.M., and Finley, L.W.S. (2019). Metabolic signatures of cancer cells and stem cells. Nat. Metab. *1*, 177–188.

Jiang, C., Jiang, L., Li, Q., Liu, X., Zhang, T., Yang, G., Zhang, C., Wang, N., Sun, X., and Jiang, L. (2019). Pyrroloquinoline quinine ameliorates doxorubicin-induced autophagy-dependent apoptosis via lysosomal-mitochondrial axis in vascular endothelial cells. Toxicology *425*, 152238.

Jiang, Y., Ji, F., Liu, Y., He, M., Zhang, Z., Yang, J., Wang, N., Zhong, C., Jin, Q., Ye, X., and Chen, T. (2017). Cisplatin-induced autophagy protects breast cancer cells from apoptosis by regulating yes-associated protein. Oncol. Rep. *38*, 3668–3676.

Kabeya, Y., Mizushima, N., Ueno, T., Yamamoto, A., Kirisako, T., Noda, T., Kominami, E., Ohsumi, Y., and Yoshimori, T. (2000). LC3, a mammalian homologue of yeast Apg8p, is localized in autophagosome membranes after processing. EMBO J. *19*, 5720–5728.

Kaushik, S., and Cuervo, A.M. (2015). Degradation of lipid droplet-associated proteins by chaperone-mediated autophagy facilitates lipolysis. Nat. Cell Biol. *17*, 759–770.

Klionsky, D.J., and Emr, S.D. (2000). Autophagy as a regulated pathway of cellular degradation. Science *290*, 1717–1721.

Komatsu, M., Waguri, S., Ueno, T., Iwata, J., Murata, S., Tanida, I., Ezaki, J., Mizushima, N., Ohsumi, Y., Uchiyama, Y., et al. (2005). Impairment of starvation-induced and constitutive autophagy in Atg7-deficient mice. J. Cell Biol. *169*, 425–434.

Lee, J.M., Wagner, M., Xiao, R., Kim, K.H., Feng, D., Lazar, M.A., and Moore, D.D. (2014). Nutrient-sensing nuclear receptors coordinate autophagy. Nature *516*, 112–115.

Lyssiotis, C.A., and Kimmelman, A.C. (2017). Metabolic interactions in the tumor microenvironment. Trends Cell Biol. *27*, 863–875.

Mauthe, M., Orhon, I., Rocchi, C., Zhou, X., Luhr, M., Hijlkema, K.J., Coppes, R.P., Engedal, N., Mari, M., and Reggiori, F. (2018). Chloroquine inhibits autophagic flux by decreasing autophagosome-lysosome fusion. Autophagy *14*, 1435–1455.

Mauvezin, C., and Neufeld, T.P. (2015). Bafilomycin A1 disrupts autophagic flux by inhibiting both V-ATPase-dependent acidification and Ca-P60A/SERCA-dependent autophagosome-lysosome fusion. Autophagy *11*, 1437–1438.

Menendez, J.A., and Lupu, R. (2007). Fatty acid synthase and the lipogenic phenotype in cancer pathogenesis. Nat. Rev. Cancer *7*, 763–777.

Mitra, R., Le, T.T., Gorjala, P., and Goodman, O.B., Jr. (2017). Positive regulation of prostate cancer cell growth by lipid droplet forming and processing enzymes DGAT1 and ABHD5. BMC Cancer *17*, 631.

Mizushima, N., and Komatsu, M. (2011). Autophagy: renovation of cells and tissues. Cell *147*, 728–741.

Mizushima, N., Levine, B., Cuervo, A.M., and Klionsky, D.J. (2008). Autophagy fights disease through cellular self-digestion. Nature *451*, 1069–1075.

Mizushima, N., Noda, T., Yoshimori, T., Tanaka, Y., Ishii, T., George, M.D., Klionsky, D.J., Ohsumi, M., and Ohsumi, Y. (1998). A protein conjugation system essential for autophagy. Nature *395*, 395–398.

Murphy, D.J. (2001). The biogenesis and functions of lipid bodies in animals, plants and microorganisms. Prog. Lipid Res. *40*, 325–438.

Nguyen, H.S., Shabani, S., Awad, A.J., Kaushal, M., and Doan, N. (2018). Molecular markers of therapy-resistant glioblastoma and potential strategy to combat resistance. Int. J. Mol. Sci. *19*, 1765.

Olzmann, J.A., and Carvalho, P. (2019). Dynamics and functions of lipid droplets. Nat. Rev. Mol. Cell Biol. *20*, 137–155.

Omuro, A., and DeAngelis, L.M. (2013). Glioblastoma and other malignant gliomas: a clinical review. JAMA *310*, 1842–1850.

Paar, M., Jungst, C., Steiner, N.A., Magnes, C., Sinner, F., Kolb, D., Lass, A., Zimmermann, R., Zumbusch, A., Kohlwein, S.D., and Wolinski, H. (2012). Remodeling of lipid droplets during lipolysis and growth in adipocytes. J. Biol. Chem. *287*, 11164–11173.

Pond, C.M. (1999). Physiological specialisation of adipose tissue. Prog. lipid Res. *38*, 225–248.

Pucer, A., Brglez, V., Payre, C., Pungercar, J., Lambeau, G., and Petan, T. (2013). Group X secreted phospholipase A(2) induces lipid droplet formation and prolongs breast cancer cell survival. Mol. Cancer *12*, 111.

Raud, B., Roy, D.G., Divakaruni, A.S., Tarasenko, T.N., Franke, R., Ma, E.H., Samborska, B., Hsieh, W.Y., Wong, A.H., Stuve, P., et al. (2018). Etomoxir actions on regulatory and memory T cells are independent of cpt1a-mediated fatty acid oxidation. Cell Metab. *28*, 504–515.e507.

Ru, P., Williams, T.M., Chakravarti, A., and Guo, D. (2013). Tumor metabolism of malignant gliomas. Cancers (Basel) *5*, 1469–1484.

Sevinsky, C.J., Khan, F., Kokabee, L., Darehshouri, A., Maddipati, K.R., and Conklin, D.S. (2018). NDRG1 regulates neutral lipid metabolism in breast cancer cells. Breast Cancer Res. *20*, 55.

Singh, R., Kaushik, S., Wang, Y., Xiang, Y., Novak, I., Komatsu, M., Tanaka, K., Cuervo, A.M., and Czaja, M.J. (2009). Autophagy regulates lipid metabolism. Nature *458*, 1131–1135.

Stupp, R., Hegi, M.E., Mason, W.P., van den Bent, M.J., Taphoorn, M.J., Janzer, R.C., Ludwin, S.K., Allgeier, A., Fisher, B., Belanger, K., et al. (2009). Effects of radiotherapy with concomitant and adjuvant temozolomide versus radiotherapy alone on survival in glioblastoma in a randomised phase III study: 5-year analysis of the EORTC-NCIC trial. Lancet Oncol. *10*, 459–466.

Sunami, Y., Rebelo, A., and Kleeff, J. (2017). Lipid metabolism and lipid droplets in pancreatic cancer and stellate cells. Cancers *10*, 3.

Talebi, A., Dehairs, J., Rambow, F., Rogiers, A., Nittner, D., Derua, R., Vanderhoydonc, F., Duarte, J.A.G., Bosisio, F., Van den Eynde, K., et al. (2018). Sustained SREBP-1-dependent lipogenesis as a key mediator of resistance to BRAF-targeted therapy. Nat. Commun. *9*, 2500.

Tauchi-Sato, K., Ozeki, S., Houjou, T., Taguchi, R., and Fujimoto, T. (2002). The surface of lipid droplets is a phospholipid monolayer with a unique Fatty Acid composition. J. Biol. Chem. *277*, 44507–44512.

Vlashi, E., Lagadec, C., Vergnes, L., Matsutani, T., Masui, K., Poulou, M., Popescu, R., Della Donna, L., Evers, P., Dekmezian, C., et al. (2011). Metabolic state of glioma stem cells and nontumorigenic cells. Proc. Natl. Acad. Sci. U S A *108*, 16062–16067.

Walther, T.C., Chung, J., and Farese, R.V., Jr. (2017). Lipid droplet biogenesis. Annu. Rev. Cell Dev. Biol. *33*, 491–510.

Wellen, K.E., and Thompson, C.B. (2010). Cellular metabolic stress: considering how cells respond to nutrient excess. Mol. Cell *40*, 323–332.

Weller, M., van den Bent, M., Hopkins, K., Tonn, J.C., Stupp, R., Falini, A., Cohen-Jonathan-Moyal, E., Frappaz, D., Henriksson, R., Balana, C., et al. (2014). EANO guideline for the diagnosis and treatment of anaplastic gliomas and glioblastoma. Lancet Oncol. *15*, e395–403.

Wen, P.Y., and Kesari, S. (2008). Malignant gliomas in adults. N. Engl. J. Med. *359*, 492–507.

iScience, Volume *23*

Supplemental Information

Lipid Droplets Maintain Energy Homeostasis and Glioblastoma Growth via Autophagic Release of Stored Fatty Acids

Xiaoning Wu, Feng Geng, Xiang Cheng, Qiang Guo, Yaogang Zhong, Timothy F. Cloughesy, William H. Yong, Arnab Chakravarti, and Deliang Guo

Supplemental Information

Transparent Methods

GBM patient samples

Autopsy and biopsy samples from GBM patients were obtained from the Department of Pathology of The Ohio State University (OSU) and University of California at Los Angeles (UCLA) Medical Center, respectively. GBM biopsies were fixed with 4% paraformaldehyde for 24 hr. One half of the biopsy was embedded in paraffin and the other half was incubated with 30% sucrose for 24 hr and further embedded in tissue-plus optimal cutting temperature (O.C.T.) compound (Cat# 23730571, Fisher). Cryosections derived from the latter were stained with BODIPY 493/503 (Cat# D-3922; Life Technologies, Grand Island, NY). The use of tissues from GBM patients was approved by the OSU and UCLA Institutional Human Care and Use Committees.

Cell lines

U87, T98, U251 GBM cell lines were cultured in Dulbecco's Modified Eagle's Media (DMEM, Cat# 15-013-CV, Corning Incorporated) supplemented with 5% FBS (Cat# SH3007103, Hyclone, GE Healthcare) in a humidified atmosphere of 5% CO_2/95% air at 37˚C. For the glucose withdrawal experiments, cells were washed once with 1x PBS and then placed into fresh DMEM medium containing 5% dialyzed FBS (Cat# 26400044, Gibco) with or without 25 mM glucose. Human astrocyte cells were maintained in Geltrex® matrix (#A1413202, Life Technologies) coated plates with DMEM supplemented with 1% of N-2 (#17502‐048, Life Technologies) and 10% of One Shot™ format FBS (#16000‐077, Life Technologies) at 37°C in a humidified atmosphere of 5% CO2. GBM patient-derived cells, GBM83, were cultured in neurobasal medium

supplemented with B-27 serum-free supplements (1x), heparin (2 mg/ml), EGF (50 ng/ml), and fibroblast growth factor (FGF, 50 ng/ml) (Ru et al., 2016).

Intracranial mouse model

Female athymic nude mice (6–8 weeks) obtained from OSU Target Validation Shared Resource were used to generate intracranial xenograft models. Cells ($1x10^5$ cells in 4 μl of PBS) were stereotactically implanted into mouse brains. Mice were observed every day and were sacrificed when they became moribund. All animal procedures were approved by the Subcommittee on Research Animal Care at Ohio State University Medical Center.

Thin-layer chromatography for lipids

TLC analysis for lipids was performed as previously described (Guo et al., 2009). Total cellular lipids were extracted by scraping cells from 10 cm culture dishes (10^6 cells) or by dissociating frozen tissues (4 mg) into 2 mL of PBS-containing protease inhibitor and 1 mM phenylmethylsulfonyl fluoride and adding 4 ml chloroform/methanol (2:1, v/v) containing 0.01% butylate hydroxytoluene (Sigma). The solution was vortexed and centrifuged at 1500x*g* for 5 min. The organic phase was collected, and 2.5 ml of chloroform was added to the remaining aqueous phase, vortexed, and centrifuged at 1500 x *g* for 5 min. The organic phase was mixed with the previous extraction. TLC was performed by spotting the cellular lipid extracts from 4 mg tissues or 10^6 cells. TG standard (Cat#10010509-1, Cayman Chemical) on a 5 cm x 10 cm silica gel aluminum sheet (Cat# 1168350001, EMD Chemicals) that was developed with hexane/diethyl ether/acetic acid (80:20:2, v/v/v). Lipids were visualized with iodine vapor and results recorded with a digital camera.

Western blotting analysis

Cultured cells were lysed and homogenized in RIPA buffer (Cat# NC9484499, Fisher Scientific) containing a phosphatase inhibitor (Cat# 04906845001, Roche), a protease inhibitor cocktail (Cat# 11836170001, Roche) and 1 mmol/L phenylmethanesulfonyl fluoride. Equal amounts of protein extracts were separated by 12% SDS-PAGE and then transferred to nitrocellulose (Cat# 162-0112, Biorad) or to PVDF membranes (Cat# 10600100, GE Healthcare) for LC3 detection. Membranes were blocked in Tris-buffered saline containing 0.01% Tween and 5% nonfat milk for 1 hr and then probed with the indicated primary antibodies, followed by the appropriate secondary antibodies (Cat #7074 or #7076; Cell Signaling) conjugated to horseradish peroxidase. The immunoreactivity was examined using the ECL kit (Cat# RPN2106, GE Healthcare). Antibodies to LC3 (Cat# 4108) and ATG5 (Cat# 8540) were purchased from Cell Signaling. Antibody to CPT1A (Cat# ab128568) was purchased from Abcam. Antibody to β-actin (Cat# A1978) was purchased from Sigma.

Cell proliferation assay

Cells ($4x10^4$) were seeded in 12-well plates and cultured overnight. Cells were washed once with 1x PBS and then placed into fresh DMEM medium supplemented with 5% dialyzed FBS (Cat# 26400044, Gibco) in the absence or presence of glucose (25 mM). Cell number was counted with a hemocytomer and cell death was determined by Trypan blue exclusion (Cat# 15250-061; Life Technologies).

Lentiviral transduction

Lentivirus vector containing ATG5 shRNA (TRCN0000330394, TRCN0000330392), CPT1A shRNA (TRCN0000036279, TRCN0000036282) and the non-mammalian shRNA control (SHC002) were purchased from Sigma. The 293FT cells were transfected with shRNA vector and packaging plasmids pCMV-R8.74psPAX2 and the envelope plasmid pMD2.G using

polyethylenimine (Cat# 23966, Polysciences). The supernatants were collected at 48 hr and concentrated using the Lenti-X Concentrator (Cat# 631232, Clontech) according to the manufacturer's protocol. Lentiviral transduction was performed according to Sigma MISSION protocol with polybrene (8 μg/mL; Cat# H9268, Sigma).

Lipid droplet staining and quantification

LDs were stained by incubating cells with 0.5 μM BODIPY 493/503 (Cat# D-3922, Life Technologies) or 0.1 μM Nile red (Cat# N1142, Life Technologies) for 30 min and visualized by confocal microscopy (Carl Zeiss LSM 510 Meta, 63x/1.4 NA oil, 1 μM wide z-stack). LDs were also detected by immunofluorescence staining with TIP47 (Cat# ab47638, Abcam). The nucleus was stained with the DAPI-containing antifade mounting reagent (Cat #P36935, Life Technologies) for tissues or fixed cells. Live cells were stained with Hoechst 33342 (5 μg/mL, 30 min) (Cat# H3570, Life Technologies) for nucleus observation. Live cells were stained with Lysotracker (Cat# L7528, Life Technologies) and Mitotracker (Cat# M2245, Life Technologies) for lysosome and mitochondrial observation, respectively. Thirty cells in each group were analyzed and particle numbers were quantified with the ImageJ software (NIH) in 3D stacks.

Immunofluorescence microscopy

Cells were seeded and cultured on glass coverslips. Cells were washed twice with 1x PBS and fixed with 4% paraformaldehyde/0.025% glutaraldehyde for 10 min followed by 5 min permeabilization with 0.1% Triton X-100. After blocking in 5% BSA for 10 min, cells were incubated with the primary antibody overnight at 4˚C, and then incubated with Alexa Fluor 488 goat anti-rabbit IgG (Cat# A-11034, Invitrogen) or Alexa Fluor 568 goat anti-rabbit IgG (Cat# A-11036, Invitrogen) for 30 min at 37˚C. Cells were then incubated with 0.5 μM BODIPY 493/503 for 30 min to stain lipid droplets. Coverslips were mounted with the antifade reagent containing

DAPI (Cat# P36935, Life Technologies) and visualized by confocal microscopy. Antibody to LC3 (Cat# 4108) was purchased from Cell Signaling, and antibody to LAMP1 (Cat# ab25630) was purchased from Abcam.

Transmission electronic microscopy (TEM)

Tumor tissues from GBM patients were first fixed in 2.5% glutaraldehyde/0.1 M phosphate (pH 7.4) for 10 min, and then cut into pieces less than 1 mm^3, followed by fixation in 2.5% glutaraldehyde/0.1M phosphate (pH 7.4) overnight at 4˚C. After fixation in 1% osmium tetroxide/phosphate buffer for 1 hr at room temperature, the tissue pieces were stained with 2% uranyl acetate/10% ethanol for 1 hr, followed by dehydration in increasing ethanol serial dilutions. The tissues were finally embedded in Eponate 12 resin. Ultra-thin sections (70 mm) were prepared on a Leica EM UC6 ultramicrotome and stained with 2% uranyl acetate and Reynold's lead citrate. TEM was performed on a FEI Tecnai G2 Spirit TEM at 80kV. Images were captured by an AMT 2 x 2 digital camera. These experiments were performed at the OSU Microscopy Core Facility.

H&E staining

Paraffin tissue sections were deparaffinized in xylene and rehydrated in decreasing ethanol serial solutions. After washing with dH_2O, slides were stained with hematoxylin and eosin solutions in sequence, followed by washing with dH_2O. Slides were then dehydrated in increasing ethanol serial dilutions, immersed in xylene and mounted in Permount™ Mounting Medium (Cat# SP15-100, Fisher Scientific).

Statistical analysis

Statistical analysis was performed in Excel and GraphPad Prism 7. Cell proliferation, quantification of LDs and TGs, and co-localization were analyzed using the two-tailed t-test as well as by ANOVA, as appropriate. $P < 0.05$ was considered statistically significant.

Figure S1

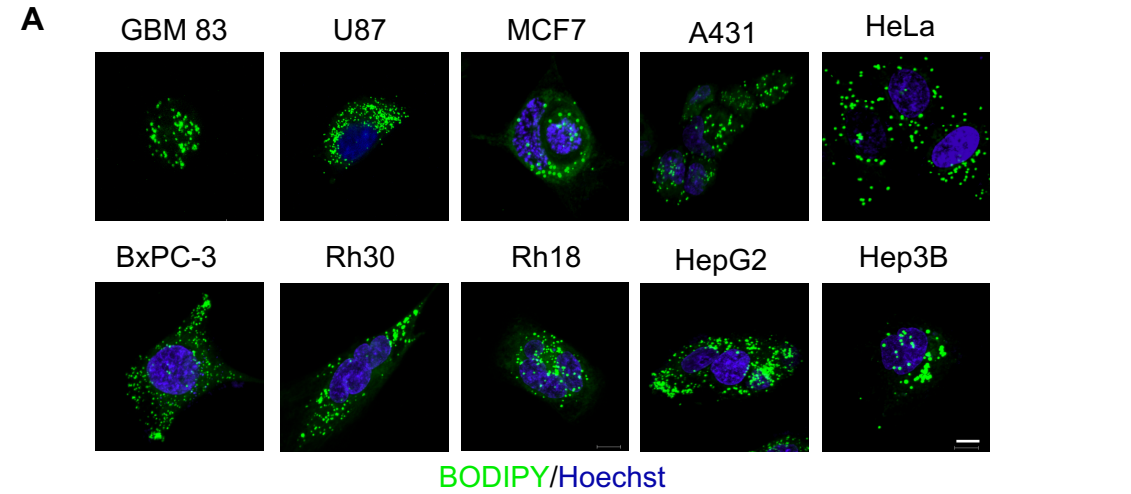
A
GBM 83
U87
MCF7
A431
HeLa
BxPC-3
Rh30
Rh18
HepG2
Hep3B
BODIPY/Hoechst

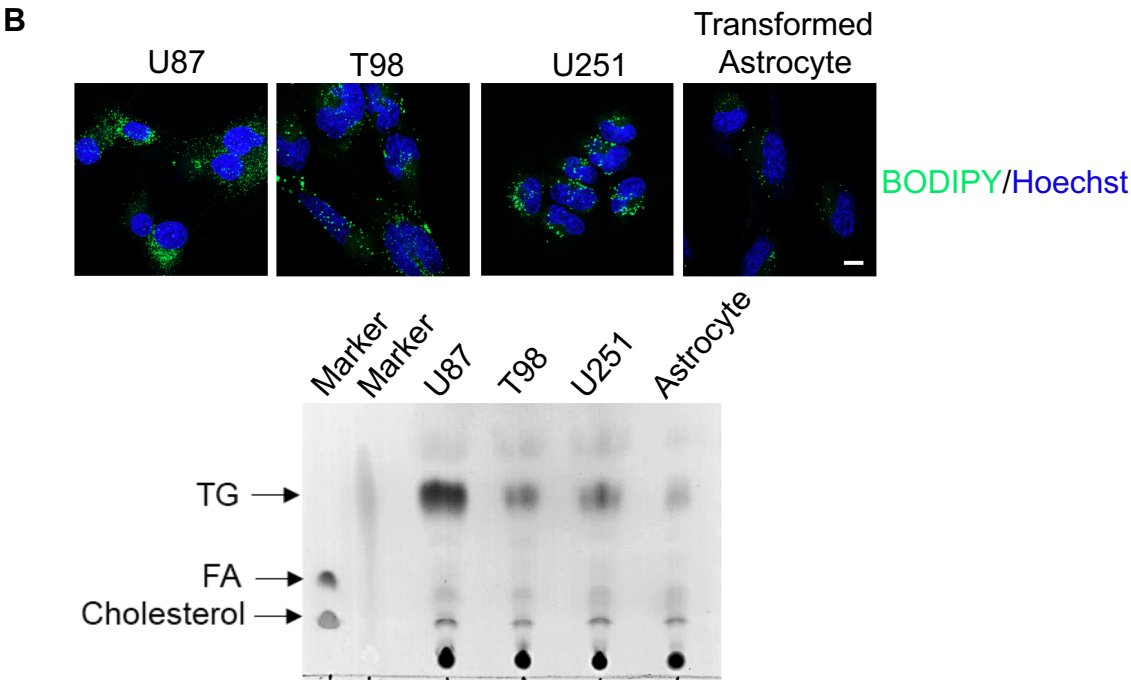
B
U87
T98
U251
Transformed Astrocyte
BODIPY/Hoechst
Marker
Marker
U87
T98
U251
Astrocyte
TG
FA
Cholesterol

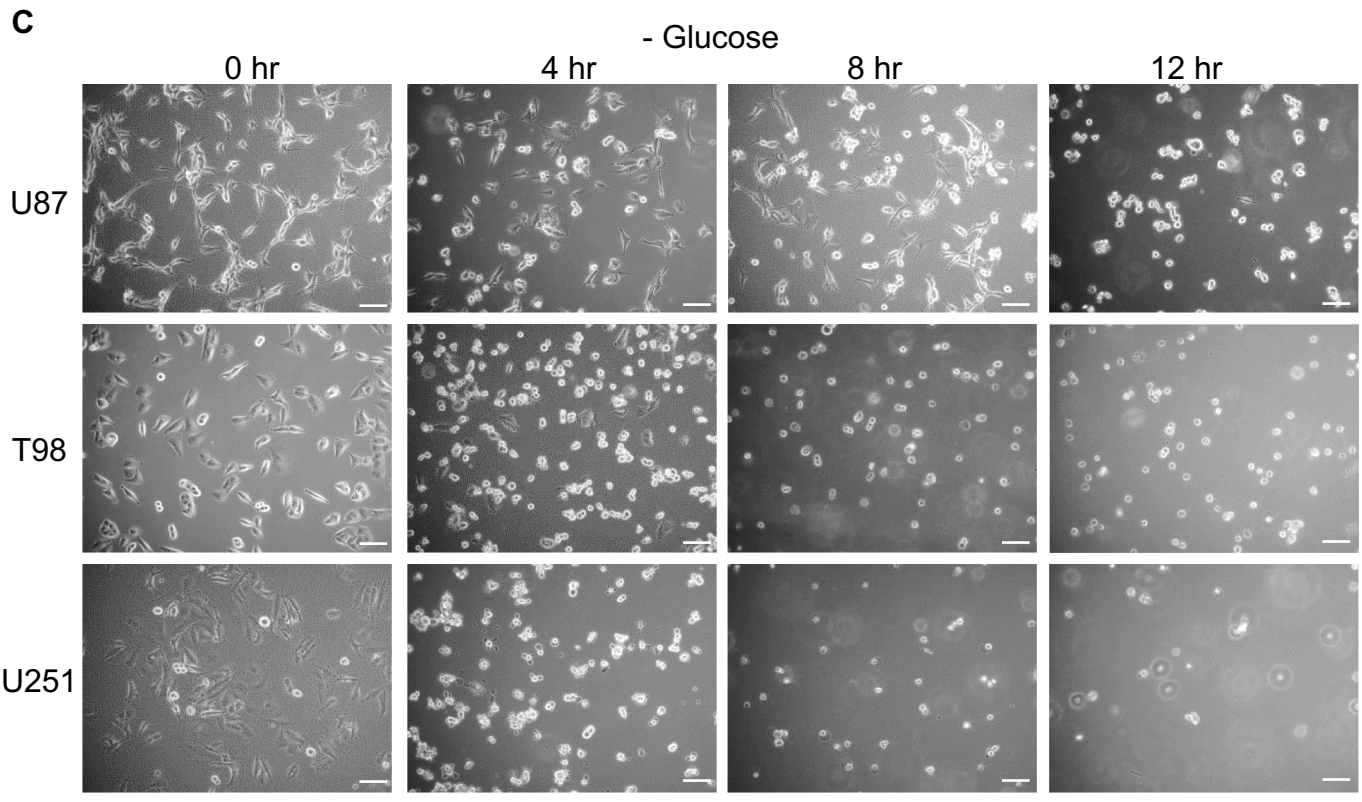
C
- Glucose
0 hr
4 hr
8 hr
12 hr
U87
T98
U251

Figure S1. Glucose withdrawal induces GBM cell death in a time-dependent manner. Related to Figures 1 and 2.

(A) Representative fluorescence images of different types of cancer cell lines stained with BODIPY 493/503 (green) and Hoechst 33342 (blue). Scale bar, 10 μm. MCF7, breast adenocarcinoma cell line; HepG2 and Hep3B hepatocellular carcinoma cell lines; A431, epidermoid carcinoma cell line; HeLa, cervical cancer cell line; BxPC-3, pancreas adenocarcinoma cell line; Rh18 and Rh30, rhabdomyosarcoma cell lines.

(B) Representative fluorescence images (upper panel) of GBM cells and transformed normal human astrocytes stained with BODIPY 493/503 (green) and Hoechst 33342 (blue). Scale bar, 10 μm. Total lipids were analyzed by TLC (lower panel). FA, fatty acids.

(C) Representative micrograph images of U87, U251 and T98 cells after withdrawal of glucose for 0 hr, 4 hr, 8 hr and 12 hr. Scale bar, 20 μm.

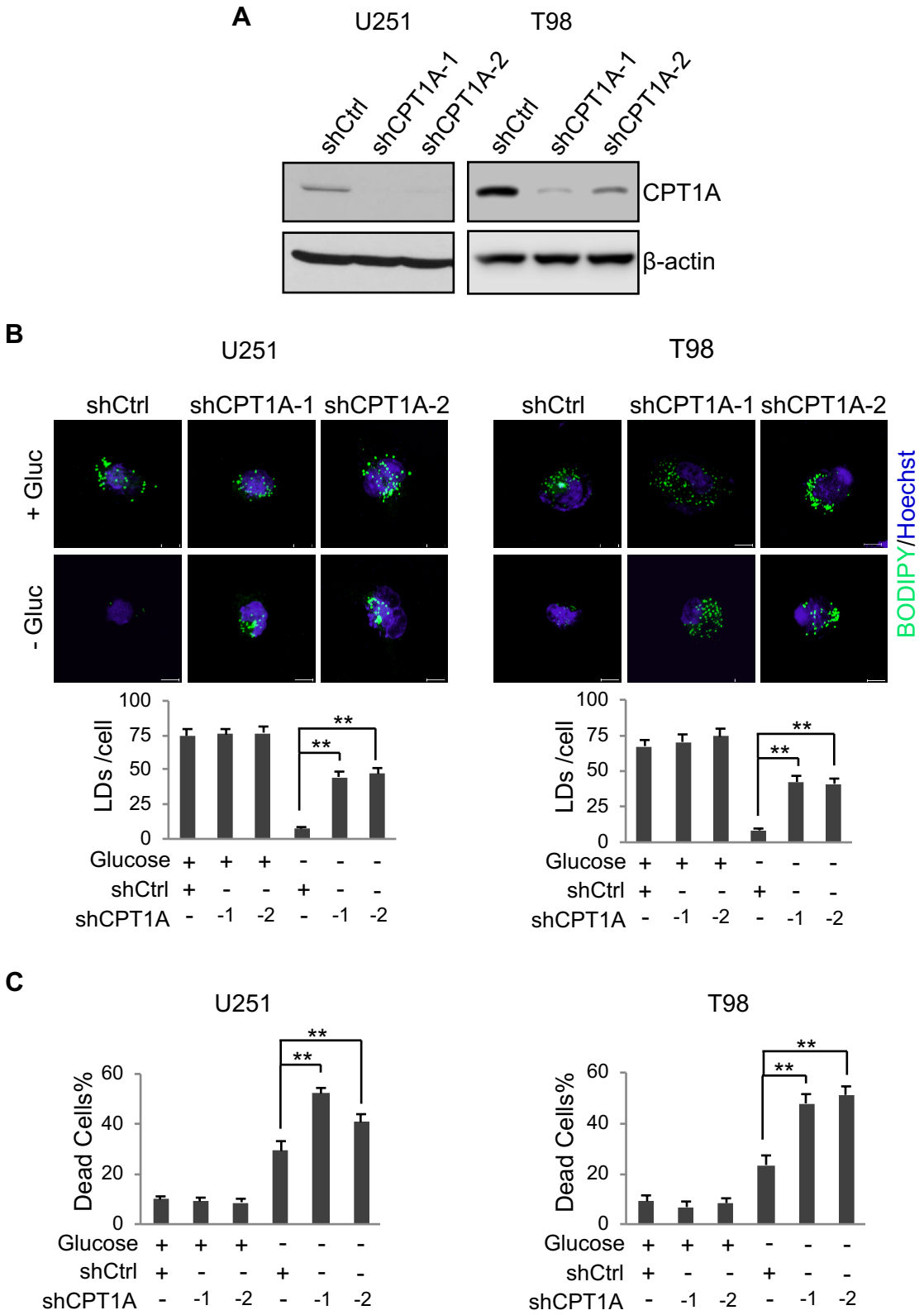

Figure S2. Genetic inhibition of CPT1A blocks glucose starvation-induced LD hydrolysis, while significantly enhancing GBM cell death. Related to Figure 3.

(A-C) U251 and T98 cells were transfected with CPT1A shRNA-expressing lentivirus for 24 hr and then cultured in glucose-free or 25 mM glucose medium for 4 hr. Cell lysates were analyzed by western blotting to determine CPT1A knockdown effects (A). The presence of lipid droplets was examined by confocal microscopy after staining with BODIPY 493/503 (green) and Hoechst 33342 (blue) (B). Quantification of LDs/cell (mean ± SEM, n = 30) was conducted using ImageJ. Cell death was determined by trypan blue staining after 3 hr glucose deprivation (mean ± SD, n = 3) (C). Significance was determined by one-way ANOVA. **p < 0.01.

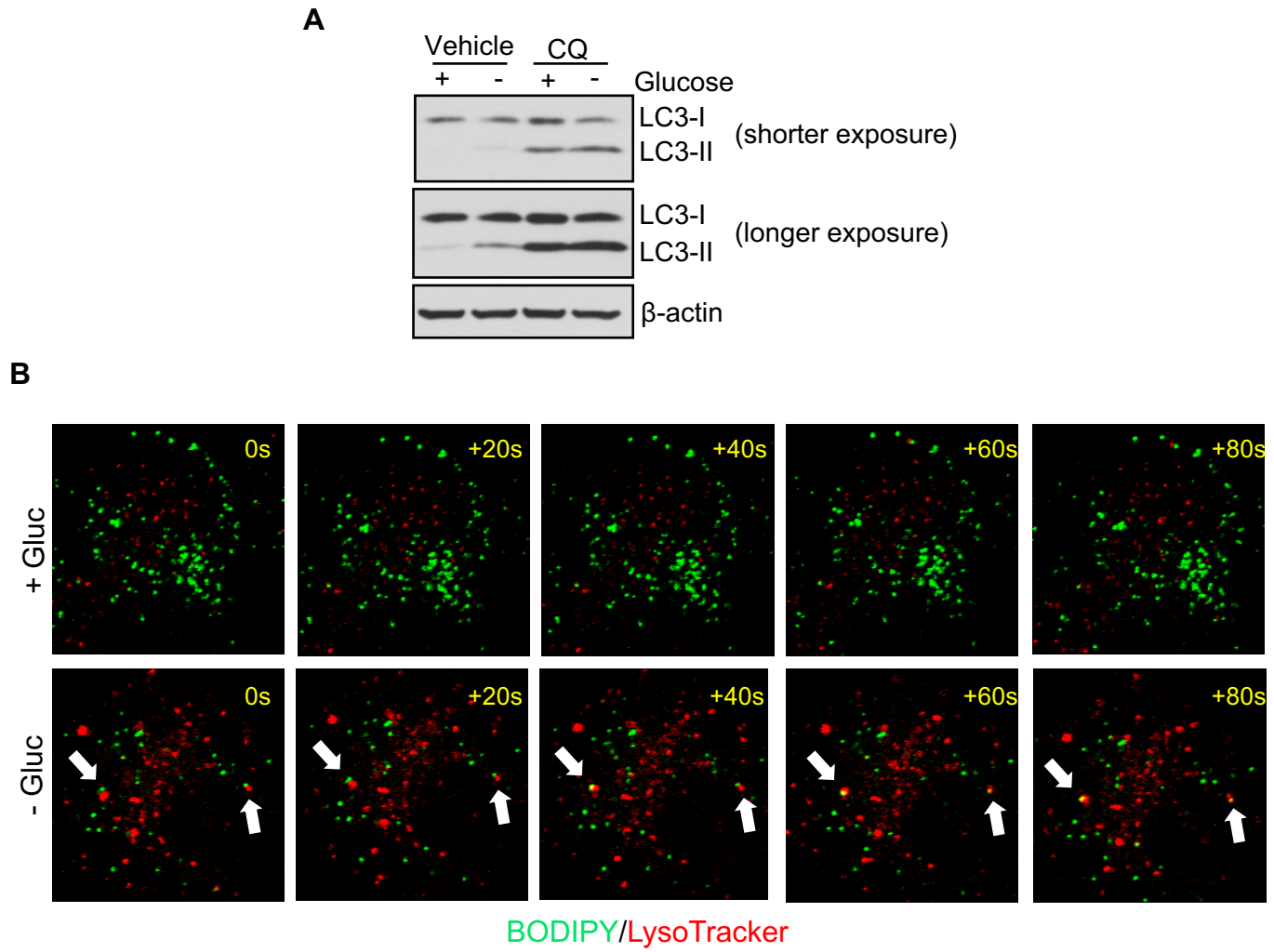

Figure S3. Glucose starvation induces autophagy to hydrolyze LDs in GBM cells. Related to Figure 4.

(A) Western blotting analysis of U87 cells in the absence or presence of glucose (25 mM) and CQ (5 μM) for 8 hr.

(B) Time-lapse imaging shows that glucose starvation induced the mobilization of LDs to the lysosomes in U87 cells. Cells were stained with BODIPY 493/503 (green) and LysoTracker (red) after glucose starvation for 7 hr and then observed by confocal microscopy in 20 sec intervals in a 5% CO_2 and 37°C chamber. Arrows indicate the mobilization and colocalization events of LDs and lysosomes.

Figure S4

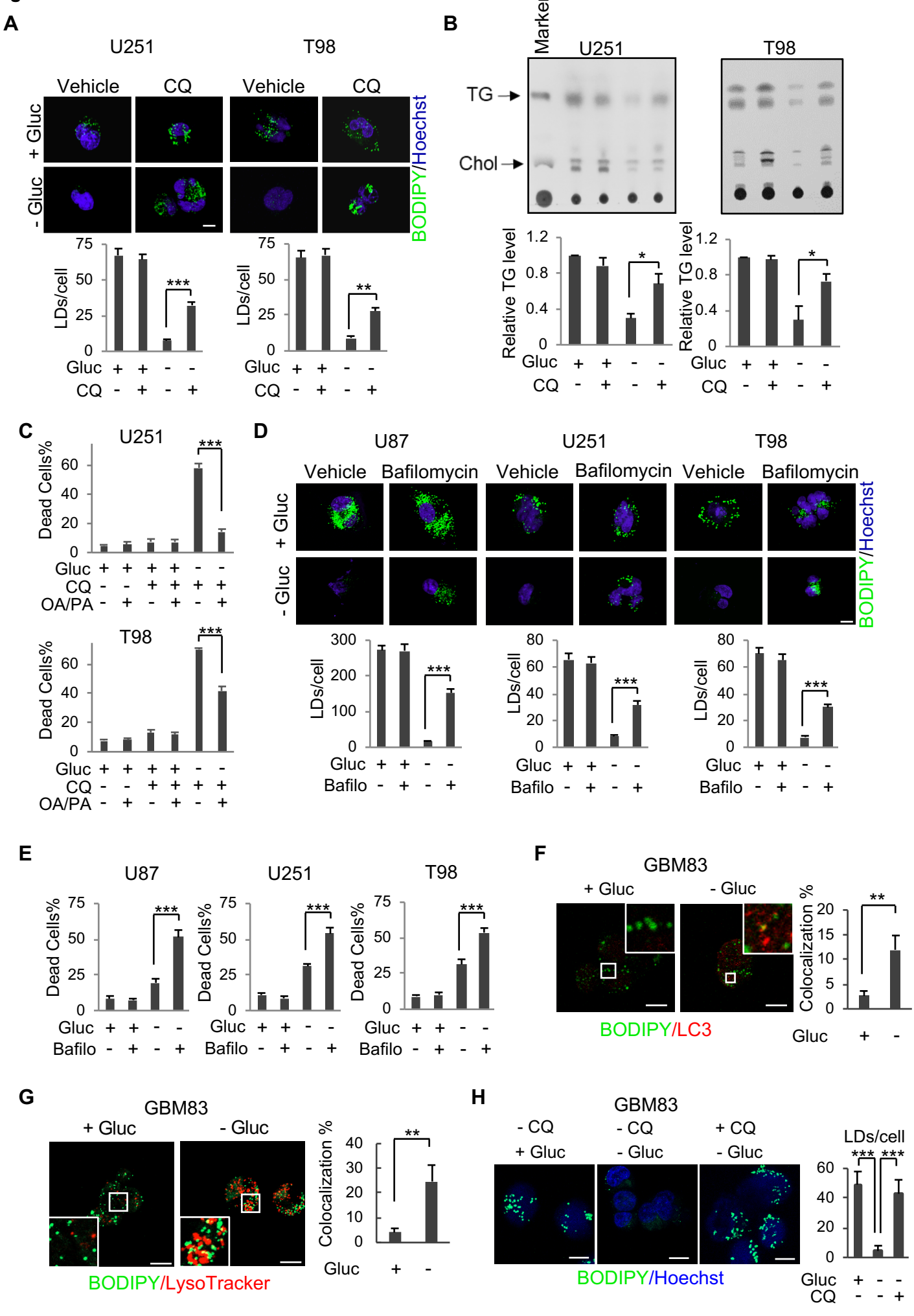
A
U251
T98
Vehicle
CQ
Vehicle
CQ
+ Gluc
- Gluc
BODIPY/Hoechst
LDs/cell
Gluc
CQ
B
Marker
U251
T98
TG
Chol
Relative TG level
Gluc
CQ
C
U251
T98
Dead Cells%
Gluc
CQ
OA/PA
D
U87
U251
T98
Vehicle
Bafilomycin
+ Gluc
- Gluc
BODIPY/Hoechst
LDs/cell
Gluc
Bafilo
E
U87
U251
T98
Dead Cells%
Gluc
Bafilo
F
GBM83
+ Gluc
- Gluc
BODIPY/LC3
Colocalization %
Gluc
G
GBM83
+ Gluc
- Gluc
BODIPY/LysoTracker
Colocalization %
Gluc
H
GBM83
- CQ
+ Gluc
- CQ
- Gluc
+ CQ
- Gluc
BODIPY/Hoechst
LDs/cell
Gluc
CQ

Figure S4. Inhibition of autophagy blocks glucose starvation-induced TG/LD hydrolysis, while significantly increasing GBM cell death. Related to Figure 4.

(A and B) U251 and T98 cells were treated with/without CQ (5 μM) in glucose-free or 25 mM glucose medium. After 4 hr, cells were stained with BODIPY 493/503 (green) and Hoechst 33342 (blue) and then observed by confocal microscopy (A). Scale bar: 10 μm. Quantification of LDs/cell (mean ± SEM, n = 30) was conducted by examining over 30 cells. Total lipids were analyzed by TLC and relative TG levels were determined by ImageJ (mean ± SD, n = 3) (B).

(C) U251 and T98 cells were cultured in medium with/without palmitic acid (PA, C16:0, 5 μM) and oleic acid (OA, C18:1, 5 μM) mixtures (1:1) for 24 hr, and then treated with/without CQ (5 μM) in the absence or presence of glucose (25 mM) for 3 hr to determine cell death by trypan blue staining (mean ± SD, n = 3) (C).

(D and E) GBM cells were treated with/without Bafilomycin (100 nM) in glucose-free or 25 mM glucose medium for 8hr (U87 cells) or 4 hr (U251 and T98 cells). Cells were stained with BODIPY 493/503 (Green) and Hoechst 33342 (blue) and then observed by confocal microscopy. Scale bar: 10 μm. Quantification of LDs/cell was determined same as in panel A. Cell death was determined by trypan blue staining after 8hr (U87) or 4 hr (U251 and T98) treatment (E).

(F and G) Representative fluorescence images of GBM patient-derived primary GBM83 cells stained with BODIPY 493/503 (green) and anti-LC3 antibody (red) (F), or LysoTracker (red) (G) in the absence or presence of glucose (5 mM) for 4 hr. The co-localization was quantified by ImageJ (mean ± SEM, n = 10 cells).

(H) GBM83 cells were treated with/without CQ (5 μM) in glucose-free or 5 mM glucose medium. After 12 hr, cells were stained with BODIPY 493/503 (green) and Hoechst 33342 (blue) and then observed by confocal microscopy. Scale bar: 10 μm. LDs/cell were quantified by ImageJ (mean ± SEM, n = 30 cells).

Significance was determined by one-way ANOVA. *$p < 0.05$, **$p < 0.01$, ***$p < 0.001$.